Dissolution of Ferrous Alloys into Molten Pure Aluminium under Forced Flow

Dissolution of Ferrous Alloys into Molten
Pure Aluminium under Forced Flow*

By Mitsuo Niinomi**, Yukinao Suzuki*** and Yoshisada Ueda****

Commercially pure iron, S45C, Fe–Cr, Fe–Si and Fe–C alloys were dipped into molten aluminium (99.8%) mostly at 1073 K and rotated at various speeds for various times. Then an alloy layer formed on each alloy was examined, and the dissolution process of these alloys was studied. The thickness of the alloy layers became thinner with increasing rotating speed. With regard to the composition of the alloy layers, Fe_2Al_5 occupied the major portion in the same manner as under the static condition. The shape of the alloy layers formed on commercially pure iron, Fe–Cr and Fe–Si alloys changed from tongue-like to band-like, as the rotating speed increased. For Fe–C alloy, the alloy layer is band-like at every rotating speed.

The dissolution rate of each alloy layer increased, as the rotating speed increased. As under the static condition, the dissolution resistance against molten aluminium is the highest in Fe–C alloy and the lowest in Fe–Si alloy. The dissolution process of commercially pure iron, S45C, Fe–Cr and Fe–Si alloys is controlled by the diffusion of Fe in molten aluminium. Moreover, in commercially pure iron, Fe–Cr and Fe–Si alloys, the dissolution is accelerated by natural convection and flaking of the alloy layer at lower rotating speed, while, at higher rotating speed, it is accelerated by flaking of the alloy layer and mechanical erosion due to molten aluminium or by turblent flow near the rugged surface of alloys. The dissolution of Fe–C alloy, however, was controlled by the chemical reaction or mass transfer in the alloy layer and the diffusion of Fe in molten aluminium.

I. Introduction

The dissolution of various ferrous alloys into static molten aluminium bath has been studied fundamentally, in order to obtain a ferrous alloy with high resistance against molten aluminium[1]–[3]. In melting and casting processes of aluminium, however, ferrous alloys are often in contact with flowing molten aluminium. Hence, the corrosion of ferrous alloy by molten aluminium under the forced flow must be discussed in detail.

As a model, the investigation on the dissolu-

tion of ferrous alloys by rotating cylindrical specimens in molten aluminium can be considered. Concerning the dissolution of solid metal into molten metal, many studies have been performed with the solid Fe–C alloy-liquid Fe–C alloy system[4]–[8], but few with the alloy system in this study[5][9][10]. Moreover, the study using ferrous alloys of various compositions for solid metal was very few.

In the present investigation, commercially pure iron, Fe–C, Fe–Si and Fe–Cr alloys were dipped into molten pure aluminium and rotated at various speeds for various times, and then the effect of the forced flow on the dissolution of ferrous alloys into molten aluminium was studied.

II. Experimental Procedure

1. Dipping and rotating of ferrous alloys

Various ferrous alloys were prepared in the same manner as in a previous report[1]. The composition of these alloys is shown in Table 1.

** School of Production Systems Engineering, Toyohashi University of Technology, Toyohashi 440, Japan.

*** Japan Nuclear Fuel Co. Ltd., Yokohama 239, Japan.

**** Department of Metallurgy, Faculty of Engineering, Nagoya University, Nagoya 464, Japan.

Table 1   Chemical composition of specimens (mass %).

Specimen	C	Si	Mn	P	S	Cr
Commercially pure iron	0.01	0.20	0.22	0.014	0.009	—
Fe–3C	2.94	0.24	0.23	0.018	0.004	—
Fe–3Si	0.033	2.91	0.22	0.002	0.005	—
Fe–3Cr	0.009	0.15	0.18	0.001	0.006	2.94
S45C	0.43	0.25	0.80	0.008	0.023	—

The specimen was attached to a rotator of changeable speed, dipped constantly by 0.03 m in depth in the center of molten pure aluminium bath (0.35 kg) at 1073 K, then took out and air cooled. The rotating speed and the dipping time were variable.

The dipping was also performed at 1023 and 973 K for only commercially pure iron. Commercial S45C which has low carbon content was also dipped at 1073 K, because the alloys except Fe–C showed a rugged surface as mentioned later.

2. Measurement of the thickness of the alloy layers

The dipping regions of the specimens were cut out with a microcutter and embeded in resin. Thereafter, the thickness of the alloy layers was measured in the same manner as in the previous paper[1].

3. Measurement of the diameter of the specimens and calculation of the corrected diameter

The diameter of the specimens was measured in the same manner as in the previous paper[1]. Since the dipped and rotated specimens showed the rugged surface generally in this work, the diameter of the specimens was estimated from the average diameter of the upper and lower halves of the dipped specimens. That is to say, the diameter was calculated by the following equations:

$$d_I = 2\sqrt{W_I/\pi L_I \rho_s}, \quad d_{II} = 2\sqrt{W_{II}/\pi L_{II} \rho_s}$$

and

$$d = (d_I + d_{II})/2,$$

where

d_I, d_{II}: average diameters of the upper or

lower halves of the specimen (m)

W_I, W_{II}: weight of the upper or lower half of the specimen (kg)

L_I, L_{II}: length of the upper or lower half of the specimen (m)

ρ_s: density of the ferrous alloy measured previously (kg/m^3)

and

d: average diameter of the specimen (m)

These calculated average diameters (d) were corrected for the weight W_I and W_{II}[1] on the assumption that Fe_2Al_5 occupied the whole alloy layer, because Fe_2Al_5 occupied the major portion of the alloy layer in this work as in the static bath[1], as is mentioned later.

4. X-ray diffraction analysis and hardness measurement of the alloy layers

For X-ray diffraction analysis, a rod sample 0.01 m in length was cut out from the dipped and rotated specimen. For EPMA analysis and hardness measurement, the remainder of the specimen was used. The subsequent procedure was carried out in the same manner as in the previous paper[1].

III.   Experimental Results and Discussion

1.   Composition of the alloy layer formed on each ferrous alloy

Figure 1 shows typical X-ray diffraction patterns of the alloy layer formed on Fe–3Cr alloy rotated at 2.67 s^{-1}. These patterns are almost in agreement with those of the alloy layer under the static condition[1].

EPMA analysis in the center of the alloy layer showed a little change in intensity of Fe– and Al–K lines, but this change did not exceed the
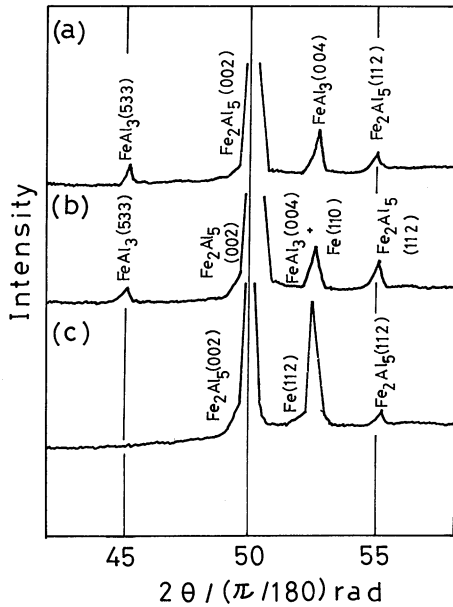
Fig. 1   X-ray diffraction patterns (Fe–3Cr alloy rotated at 2.67 s⁻¹ in molten pure aluminium at 1073 K).
(a)   Surface of the alloy layer.
(b)   Center of the alloy layer.
(c)   Alloy layer near the base iron.

Table 2   Al/(Fe·M) atomic ratio of the alloy layer obtained by EPMA analysis.

Specimens, Dipping temp. Rotating speed, Dipping time	Al/(Fe·M)	
	Under the forced flow	†Under the static[1] condition
Commercially pure iron, 1073 K, 2.63 s⁻¹, 0.6 ks	2.2	
Commercially pure iron, 1073 K, 5.18 s⁻¹, 0.9 ks	2.5	2.7
Commercially pure iron, 973 K, 2.67 s⁻¹, 1.5 ks	2.3	
Commercially pure iron, 973 K, 4.72 s⁻¹, 1.2 ks	2.2	2.8
Fe–3C, 1073 K, 2.63 s⁻¹, 1.2 ks	2.8	
Fe–3C, 1073 K, 5.22 s⁻¹, 1.2 ks	2.4	2.4–2.5
Fe–3Cr, 1073 K, 2.67 s⁻¹, 0.6 ks	2.4	
Fe–3Cr, 1073 K, 4.72 s⁻¹, 0.9 ks	2.7	2.5
Fe–3Si, 1073 K, 2.67 s⁻¹, 0.6 ks	2.4	2.3

†   In the case of static condition, the dipping time differs from that in the case of forced flow.

limit within which the concentrations could be considered almost constant. Therefore, Al/(Fe·M) atomic ratios (M: the third element) of the alloy layers, obtained in the same manner as in the previous paper[1], are given in Table 2 with those under the static condition. These values are in the range from FeAl₃ to Fe₂Al₅ phases which exist at room temperature in the Fe–Al phase diagram[11]. Most values indicate Fe₂Al₅ phase. The distribution of alloying elements dissolved into the alloy layers was examined by EPMA line analysis. It was found that Cr was dissolved to some extent in the alloy layer of Fe–3Cr alloy.

Hardness measurement indicated that the hardness of the alloy layer almost coincided with that of FeAl₃ to Fe₂Al₅ phase[12].

These results are almost in agreement with those in the static bath. The alloy layer formed on each ferrous alloy is mostly FeAl₃ near the base metal, while Fe₂Al₅ occupied the major portion of the alloy layer.

2.   Metallographic observation of the alloy layers

In the static pure aluminium bath[1], the alloy layers formed on commercially pure iron, Fe–3Cr and Fe–3Si alloys were markedly tongue-like, and that formed on Fe-3C alloy was almost band-like and slightly tongue-like at the tip. However, under the forced flow, as shown in Fig. 2 and Fig. 3, the alloy layers on commercially pure iron, Fe–3Cr and Fe–3Si alloys changed from tongue-like to band-like, as the rotating speed increased. The alloy layer on Fe–3Si alloy approached the band-like shape at a rotating speed lower than those for commercially pure iron and Fe–3Cr alloy. For Fe-3C alloy, the shape of the layer did not change and was band-like similar to that in the static condition, even if the rotating speed increased.

For the static bath, a narrow range of Fe–Al solid solution existed inside the tongue-like Fe₂Al₅ phase in commercially pure iron, Fe–3Cr and Fe–3Si alloys. Such a solid solution was also observed at lower rotating speed, but not at higher rotating speed.

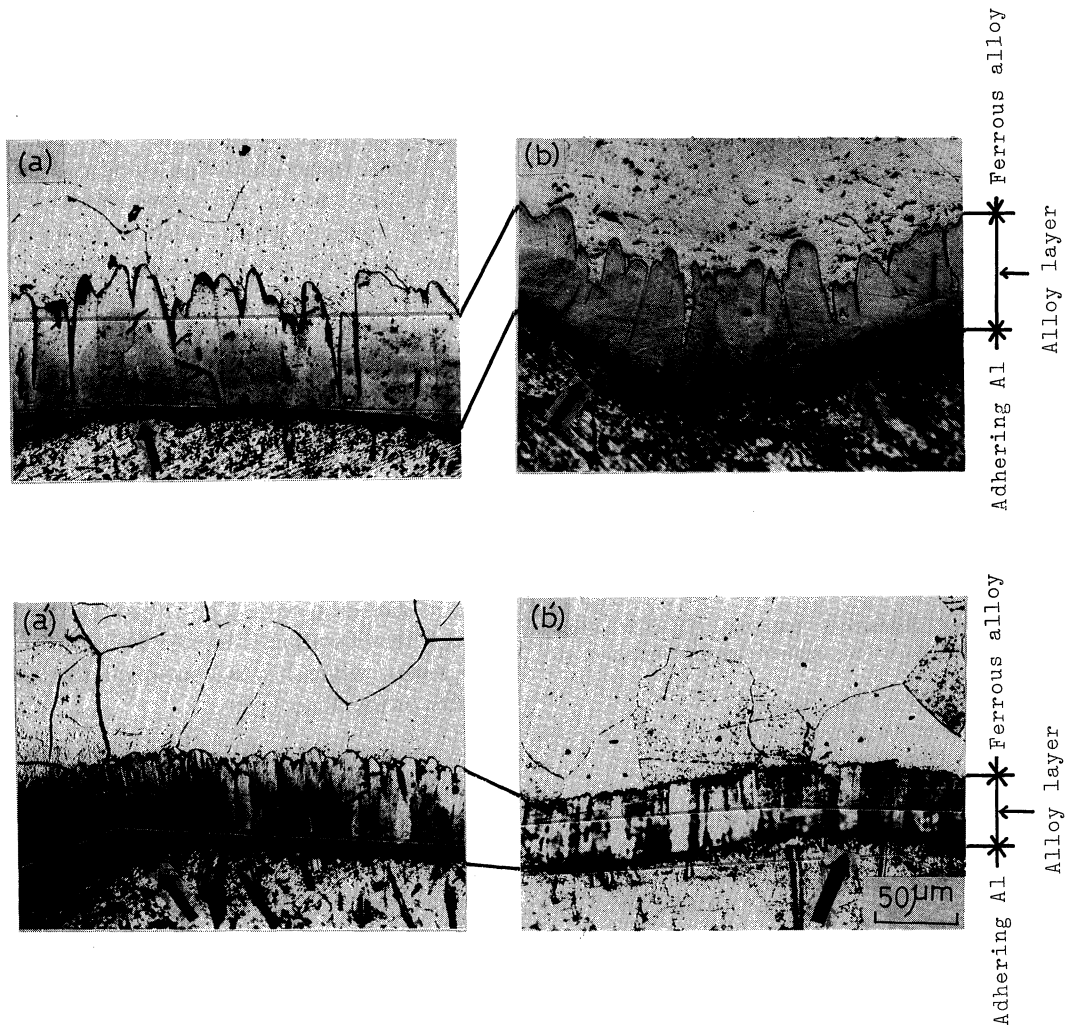The shape of the alloy layer near the adhering

Fig. 2   Alloy layers formed on commercially pure iron and Fe–3Cr alloy rotated in molten pure aluminium at 1073 K.
   (a)   Commercially pure iron, rotated at 2.63 s^{-1} for 600 s.
   (a′)   Commercially pure iron, rotated at 13.63 s^{-1} for 300 s.
   (b)   Fe–3Cr alloy, rotated at 2.67 s^{-1} for 300 s.
   (b′)   Fe–3Cr alloy, rotated at 13.63 s^{-1} for 300 s.

aluminium was flat in the static bath, but rugged for the rotated specimens, as shown by the arrow in Fig. 1 and Fig. 2. The rugged shape may be an evidence of flaking of the alloy layer. However, this phenomenon cannot be observed for Fe–3C alloy.

3.   Growth of the alloy layers

Figure 4 shows the relation between the thickness of the alloy layer and the dipping time for commercially pure iron as a typical example.

The thickness of the alloy layers decreased with increasing rotating speed for almost all specimens. The tendency that the thickness increases with dipping time as observed in the static bath[1] could not be observed.

The differences in the thickness of the alloy layers among the specimens, and among the temperatures for commercially pure iron are shown in Fig. 5 at rotating speed of 2.67 s^{-1}. The alloy layer of Fe–3Si alloy was considerably thinner than the other alloys. The difference
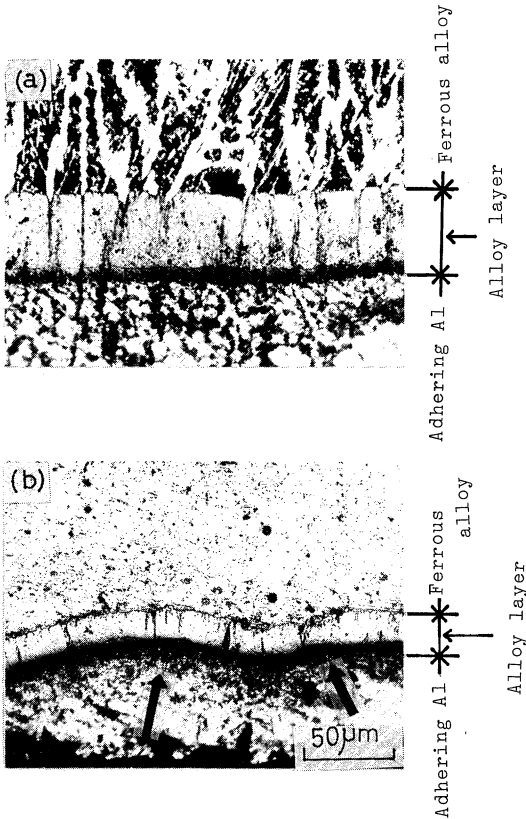
Fig. 3 Alloy layers formed on Fe–3C and Fe–3Si
alloys rotated in molten pure aluminium at 1073 K.
(a) Fe–3C alloy, rotated at 2.67 s⁻¹ for 1200 s.
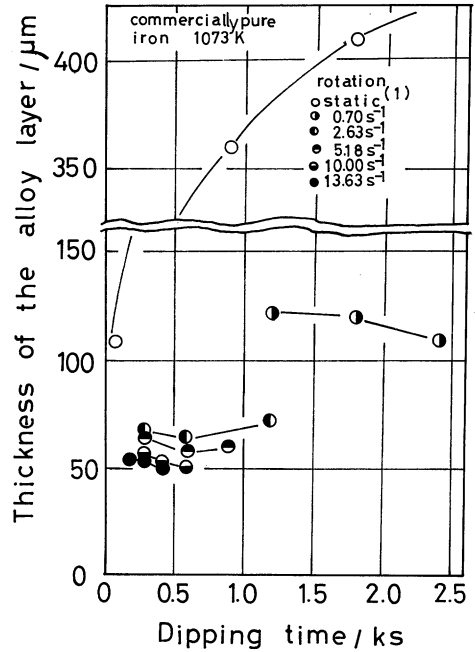(b) Fe–3Si alloy, rotated at 2.67 s⁻¹ for 600 s.

Fig. 4 Relation between thickness of the alloy layer
and dipping time.

Fig. 5 Relation between thickness of the alloy layer
and dipping time and temperature.

among the other alloys, however, was rather
small in comparison with the large difference
observed in the case of static bath[1]. The differ-
ence in the thickness of the alloy layers among
temperatures for commercially pure iron could
be hardly observed at the same rotating speed.

When ferrous alloys are rotated, the amount
of dissolution increases as mentioned later. As a
result, the alloy layers become thinner and ap-
proach the band-like shape. Moreover, for
commercially pure iron and Fe–Si alloy, the
decrease of the thickness of the alloy layer may
be enhanced by flaking.

4. Decreasing amount of the corrected diameter of ferrous alloys

Figure 6 shows the change in the corrected
diameter with dipping time and rotating speed
for Fe–3Cr alloy, where the result under the

static pure Al-bath is added. The decreasing
amount of the corrected diameter of ferrous
alloys increases, as the rotating speed increases
linearly with dipping time. But, in the static
bath, the corrected diameter decreased linearly
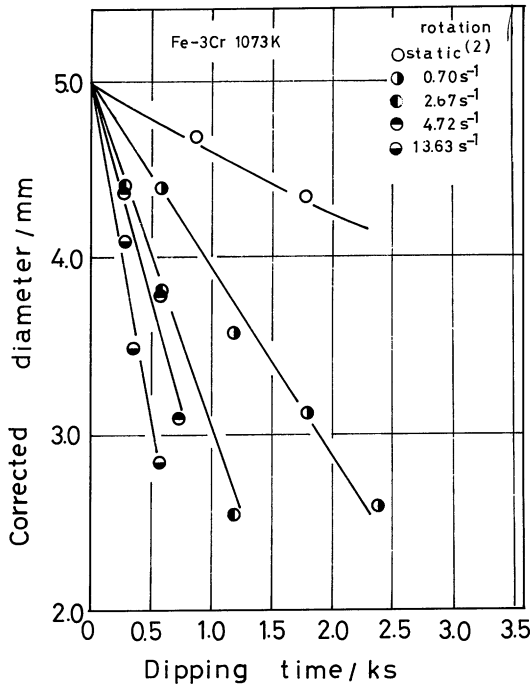with dipping time only for Fe–3Si alloy.

Fig. 6 Relation between corrected diameter and dipping time.

5. Dissolution process of each ferrous alloy

(1) Correlative equation of mass transfer under the forced flow

When dissolution of solid into liquid is controlled by the diffusion of solute element in the liquid, mass transfer between solid and liquid under the forced convection can be expressed by the following non-dimensional correlative equation:

$$J_D = (k_c/u)(Sc)^a = c.(Re)^{-b}, \qquad (1)$$

where

J_D: J_D factor
k_c: mass transfer coefficient (m/s)
u: relative velocity between solid and liquid (m/s)
Sc: Schmidt number $(Sc = \mu/\rho_1 D)$
Re: Reynolds number $(Re = L_d u \rho_1/\mu)$
a, b, c: constants
L_d: characteristic length (m) (corrected diameter)
μ: viscosity coefficient (kg/m·s)
ρ_1: density of liquid (kg/m^3)
and
D: diffusion coefficient (m^2/s)

This non-dimensional correlative equation can be applied not only to flat plate and cylindrical models but also to various models such as rotated, oval, prismatic and cubic models. Furthermore, the equation can be used for liquid metal in the same manner as for usual viscous fluid[13].

Various non-dimensional correlative equations as mentioned above were reported by experimental investigations on mass transfer between solid and liquid using a rotated cylinder. Typical examples are as follows:

$$J_D = (k_c/u)(Sc)^{0.644} = 0.0791(Re)^{-0.30}, \qquad (2)$$

where $Re = 150 - 52000$ and $Sc = 835 - 11000$,

for benzonic acid and -water and -glycerin by Eisenberg et al.[14]

$$J_D = (k_c/u)(Sc)^{0.60} = 0.135(Re)^{-0.4}, \qquad (3)$$

where $Re = 200 - 2.5 \times 10^5$ and $Sc = 462 - 31200$,

for benzonic acid -water and -sucrose solution by Bennet and Lewis[15].

$$J_D = (k_c/u)(Sc)^{0.644} = 0.112(Re)^{-0.330}, \qquad (4)$$

where $Re \fallingdotseq 900 - 40000$,

for steel cylinder-molten iron (Fe–C) by Kim and Pelke[7].

$$J_D = (k_c/u)(Sc)^{2/3} = 0.12(Re)^{-0.31}, \qquad (5)$$

where $Re = 29 - 260$,

for solid MgO-molten Fe$_t$O–CaO–SiO$_2$ slag by Umakoshi et al.[16]

$$J_D = 0.83Re^{-0.5} \quad \text{(laminal flow region)} \qquad (6)$$

for solid lime-molten CaO–Al$_2$O$_3$–SiO$_2$ slag by Kawai[17].

Besides, the correlative equation for benzonic acid-water $(Re = 50 - 34700, Sc = 942)$ was reported by Sherwood and Ryan[18], which was in good agreement with that by Eisenberg et al.[14]

Smith and Greif[19] reported the following correlative equation by a theoretical study:

$$Sh = 3K \cdot 3^{2/1}/2\pi \cdot (f/2)^{1/2}$$
$$\cdot (Sc/Sc_t)^{1/3}(1 + 4\beta/Re \cdot 2f)^{1/3}, \qquad (7)$$

where
Sh: Sherwood number $(Sh = L_d k_c'/D)$
k_c': mass transfer coefficient (cm/s)
K: constant (7.47×10^{-2})

β: constant $(=5)$

f: friction coefficient $(f/2=0.079(Re)^{-0.30})$

and

Sc_t: Schmidt number for turbulent flow $(=1.0)$

J_D value can be obtained by changing this theoretical equation.

J_D values calculated by the above correlative equations are plotted against Re number. Then, the dissolution process of ferrous alloys can be discussed by comparing J_D values obtained in this study, which is called J_{ob} hereafter, with the calculated J_D values.

(2) Calculation of J_{ob} values in this study

In order to estimate J_{ob} values, the apparent mass transfer coefficient k_{ob} (equivalent to k_c or k'_c in the equations), the relative velocity u, Schmidt number Sc and the constant a must be estimated, as shown in eq. (1).

As described by the static bath[2], when the dissolution of solid specimen is controlled by mass transfer in molten metal, k_{ob} can be ob-

tained by the following equation:

$$k_{ob} = -r_1 \cdot \rho_s (dr_1/dt)$$
$$/(\%x_{1s} \cdot \rho_{1s}/100 - \%x \cdot \rho_1/100)r_2,$$

where

r_1: corrected radius (one-half of corrected diameter) (m)

r_2: distance from the center of the specimen to the surface of the alloy layer (m)

$\%x$: solute concentration in molten metal (mass %)

ρ_1: density of molten metal (kg/m^3)

$\%x_{1s}$: saturated solute concentration in molten metal (mass %)

and

ρ_{1s}: density of molten metal saturated with solute (kg/m^3)

The relative velocity u (m/s) can be calculated by the equation, $u=2\pi r_2 R$, where R is the rotating speed of specimen per second (s^{-1}).

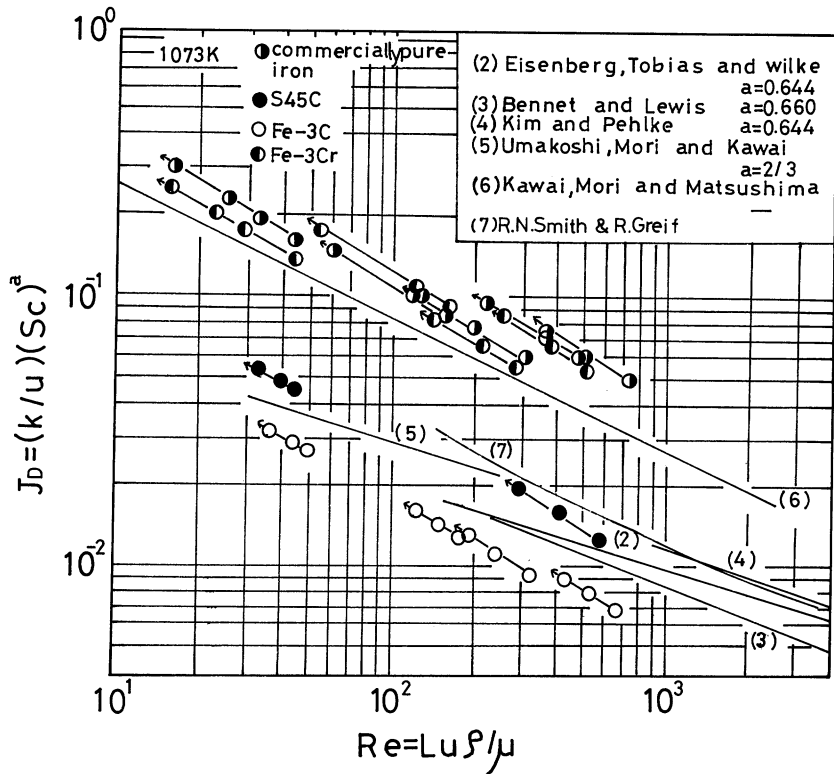The constant a is 1/3–2/3 for various models

Fig. 7 Non-dimentional correlation of mass-transfer from rotated solid ferrous alloy into molten pure aluminium bath.

and systems, and $a=2/3$ is adopted in this experiment.

The diffusion coefficient, the density and the viscosity of molten aluminium are required in order to calculate Sc number. The values used for the discussion on the static bath are adopted[20]-[22] for the calculation of Re number in this study. For $\%x_{1s}$, the value in the previous paper[23] is also used.

(3) Discussion on controlling step of dissolution of ferrous alloys

J_{ob} values obtained in this study are plotted against Re number in Figs. 7 and 8. Figure 7 shows the results of commercially pure iron, Fe–3C and Fe–3Cr alloys at 1073 K, and Fig. 8 shows the results of Fe–3Si at 1073 K and commercially pure iron at 1023 and 973 K. The results of S45C at 1073 K are given in both figures. The values obtained by the non-dimensional correlative equation shown in 5.(1) are also given. The exponent of Sc number

in J_D factor is expressed by a. J_D changes with time, and the time progress is expressed by the arrow. The exponent of Sc number in each equation is not always 2/3, but this value may be used for the purpose of comparison and discussion, because the accuracy of each physical property is not high.

When the non-dimensional correlative equations shown in these figures are compared among one another, eqs. (2), (3), (4) and (5) are in good agreement, but eq. (6) gives a considerably higher J_D value. Many other papers report the equations which are also in good agreement with eqs. (2), (3), (4) and (5)[5][24][25]etc.. Furthermore, these equations agree also with the theoretical correlative eq. (7). Therefore, eqs. (2)–(7) may be considered as the standard. If the experimental values agree with these equations, the dissolution of ferrous alloy can be considered to be controlled by the diffusion process that Fe atoms diffuse through the diffusion layer into bulk in molten pure
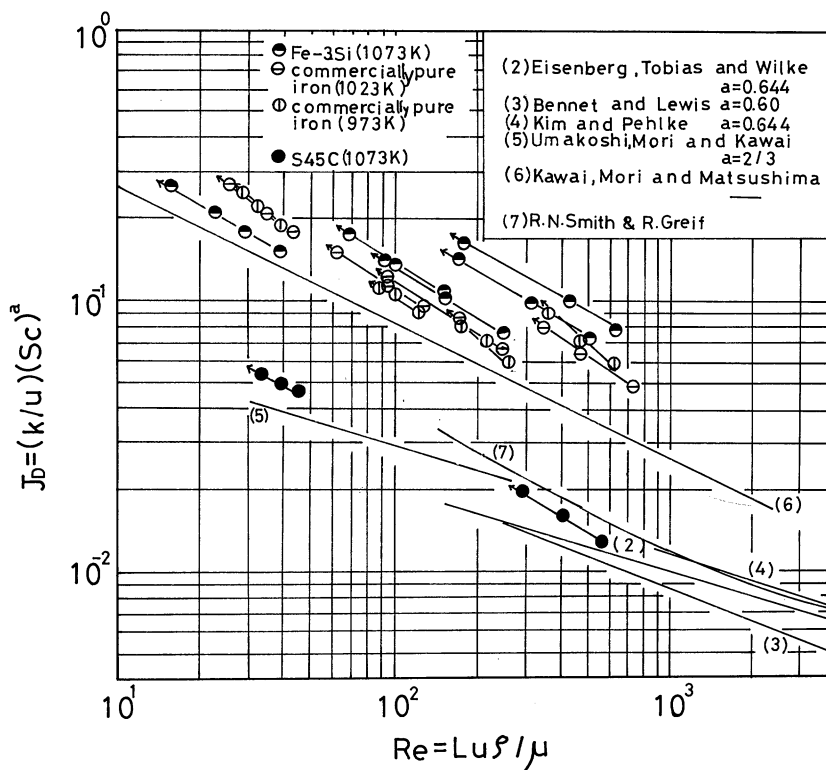

Fig. 8   Non-dimensional correlation of mass-transfer from rotated solid ferrous alloy into molten pure aluminium bath.

aluminium. If the experimental values are considerably lower, processes such as the reaction at the interface between ferrous alloy layers, the diffusion process of Fe in the alloy layer and the formation process of alloy layer, or the reaction at the interface between alloy layer and molten aluminium are the controlling step of dissolution.

In this experiment, the alloy layers of commercially pure iron, Fe–3Cr and Fe–3Si alloys flaked off as mentioned above. Moreover, the rugged surface was observed for these specimens inside the alloy layers rotated at more than 2.67 s^{-1}. But this phenomenon was not observed for Fe–3C alloy. Then a rather lower carbon alloy, S45C, was dipped and rotated, but the rugged surface was not observed on the alloy layer (Fig. 9) and also inside the alloy layer (Fig. 10). For S45C, J_{ob} was plotted against Re number (Fig. 7 or Fig. 8), which agreed well with the non-dimensional correlative equations. When rotated at 0.70 s^{-1}, J_{ob}

Fig. 9 Alloy layer formed on S45C rotated at 10.0 s^{-1} in molten pure aluminium at 1073 K.

Fe-3C	S45C	Fe-3Si
13.33 s^{-1}	10.0 s^{-1}	10.0 s^{-1}
1.8 ks	1.2 ks	0.42 ks

Fig. 10 Surface of the ferrous alloy inside the adhering aluminium and alloy layer.

was slightly higher, which will be mentioned later.

(a) Dissolution of S45C

When S45C was rotated at 10 s^{-1}, as shown in Figs. 7 or 8, J_{ob} was in good agreement with the non-dimensional correlative equations. When rotated at 0.70 s^{-1}, the specimen was more attacked at its upper portion than at its lower portion. This is an evidence of the effect of natural convection[2][5]. Therefore, J_{ob} at 0.70 s^{-1} can be considered to become greater than J_D of the non-dimensional correlative equation. As J_{ob} of S45C is in good agreement with J_D of the correlative equation, the dissolution of S45C is considered to be controlled by the diffusion of Fe atoms in molten aluminium.

The mass transfer resistance or the chemical reaction resistance was considered to exist in the alloy layer for the dissolution of commercially pure iron and Fe–C alloys (2% and 3%C) in the static bath[2]. Hence, such a resistance can be also considered to exist in the alloy layer of S45C. But this is negligible because of considerably thin alloy layer. So, S45C can be considered as a standard for the discussion about the controlling step of dissolution of the other alloys.

(b) Dissolution of commercially pure iron, Fe–3Cr and Fe–3Si alloys

By the dissolution of commercially pure iron and Fe–3Cr alloy in the static bath[2], it is clear that the alloy layer was thick, and the mass transfer resistance or the chemical reaction resistance was considered to exist in the alloy layer. However, the alloy layers become thinner for the rotated samples, and J_{ob} is much greater than J_D of the non-dimensional correlative equation and J_{ob} of S45C. Therefore, in this case, the mass transfer resistance in the alloy layer can be considered negligible.

For Fe–3Si alloy, the mass transfer resistance or the chemical reaction in the alloy layer could be neglected in the static bath. Moreover, when rotated, J_{ob} of dissolution is greater than J_D and J_{ob} of S45C. Therefore, for this alloy, the mass transfer or the chemical reaction resistance in the alloy layer can be considered negligible.
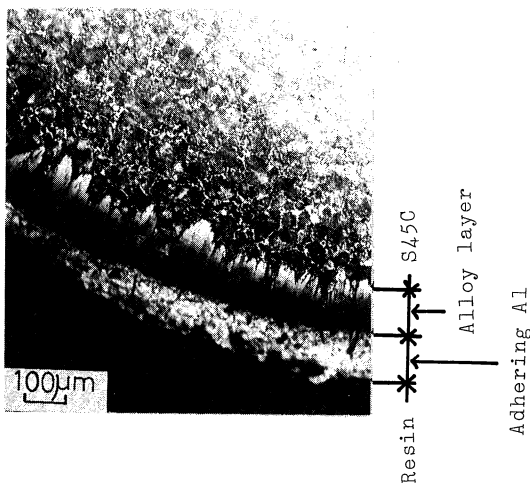
As mentioned above, the dissolution of commercially pure iron, Fe–3Cr and Fe–3Si alloys under the rotation is considered to be controlled by diffusion of Fe atoms in molten aluminium. However, J_{ob} values of these alloys are considerably larger. So, a factor, which accelerates the dissolution, must be considered, other than the decrease of thickness of the alloy layer by the rotated specimen.

As mentioned above, by these alloys, some trace of flaking of the alloy layer is observed at every rotating speed. Moreover, for rotating speed $0.70~s^{-1}$, the effect of natural convection is recognized. At higher speed, the surface inside the alloy layer become rugged, and this tendency becomes more noted with increasing speed. This ruggedness is more remarkable for Fe–3Si alloy than for commercially pure iron and Fe–3Cr alloy at rapid rotation. Therefore, the rugged surface may be considered as the trace of erosion of the ferrous alloys by molten aluminium. Furthermore, it can be also suspected that a local turbulent condition in the preferentially dissolved region or a mutual effect of turbulent flow in the eroded region becomes remarkable with increasing rotating speed.

The dissolution process will be discussed now by contrasting this phenomenon with J_{ob} values. J_{ob} values at a low rotating speed become very large, when the dissolution is accelerated by the nautral convection or flaking of the alloy layer. As rotating speed increases, J_{ob} values of Fe–3Si alloy become larger than those of commercially pure iron and Fe–3Cr alloy. The tendency is in agreement with the increasing ruggedness. Therefore, at a high rotating speed, the dissolution may be accelerated by flaking of the alloy layer and erosion of the ferrous alloy by molten aluminium or by local turbulent condition on the rugged site.

(c) Dissolution of Fe–3C alloy

J_{ob} of Fe–3C alloy was slightly smaller than that of S45C. Hence, the mass transfer resistance or the chemical reaction resistance in the alloy layer can be considered to exist. Rotation of the specimen decreases the thickness of the alloy layer considerably, and the mass transfer resistance in the alloy layer decreases some-

what, but not negligibly. The chemical reaction resistance may exist at the interface of Fe–3C alloy and alloy layer, because of the existence of much eutectic cementite. Therefore, for the dissolution of Fe–3C alloy, a little mass transfer or chemical reaction resistance can be considered to exist in the alloy layer.

IV. Conclusion

In order to study the dissolution of ferrous alloys into molten aluminium under the forced flow, commercially pure iron, S45C, Fe–3Cr, Fe–3Si and Fe–3C alloys were dipped and rotated in molten pure aluminium, and the dissolution process of each ferrous alloy was examined. The following results were obtained.

(1) The alloy layer becomes thinner with increasing rotating speed, and the thickness is constant for various dipping times. The shape of the alloy layers formed on commercially pure iron, Fe–3Cr and Fe–3Si alloys changes from tongue-like to band-like, as the rotating speed increased. For Fe–3C alloy, the alloy layer is band-like with a slightly tongue-like tip at every rotating speed.

(2) With regard to the composition of the alloy layer, Fe_2Al_5 occupies the major portion in the same manner as under the static condition.

(3) The dissolution rate of each alloy into molten pure aluminium increases with increasing rotating speed. The corrosion resistance against molten aluminium is the highest for Fe–3C alloy and the lowest for Fe–3Si alloy. This result agrees with the tendency in the static bath.

(4) The dissolution of commercially pure iron, S45C, Fe–3Cr and Fe–3Si alloys is controlled by the mass transfer of Fe in molten aluminium. At lower rotating speed the dissolution is accelerated by natural convection and flaking of the alloy layer, while at higher rotating speed the dissolution is accelerated by flaking of the alloy layer and erosion by molten aluminium or by turbulent flow at the rugged site on the alloy surface.

In the alloy layer of Fe–3C alloy, there may be a little mass transfer or chemical reaction resistance in the molten aluminium under the

forced flow condition as well as under the static condition.

Acknowledgements

REFERENCES

(1) M. Niinomi and Y. Ueda: Trans. JIM, **23** (1982), 709.

(2) M. Niinomi, Y. Ueda and M. Sano: Trans. JIM, **23** (1982), 780.

(3) Y. Ueda and M. Niinomi: J. Japan Foundrymen's Soc., **50** (1978), 549 (in Japanese).

(4) M. Kosaka and S. Minowa: J. Iron Steel Inst. Japan, **53** (1967), 983 (in Japanese).

(5) M. Kosaka and S. Minowa: J. Iron Steel Inst. Japan, **52** (1966), 1748 (in Japanese).

(6) H. Nomura and K. Mori: J. Iron Steel Inst. Japan, **55** (1969), 1134 (in Japanese).

(7) Yeng.U Kim and R. D. Pelke: Met. Trans., **5** (1974), 2527.

(8) T. Sakurai and K. Mori: J. Iron Steel Inst. Japan, **62** (1976), S568 (in Japanese).

(9) S. Minowa and M. Kosaka: J. Iron Steel Inst. Japan, **50** (1964), 56 (in Japanese).

(10) J. A. Leak: Acta Crystallogr, **17** (1964), 56.

(11) M. Hansen: *Constitution of Binary Alloys*, McGraw-Hill, (1958), p. 90.

(12) K. Nishida and T. Narita: J. Japan Inst. Metals, **35** (1970), 269 (in Japanese).

(13) A. Hirata: Chemical Engineering, **28** (1964), 102 (in Japanese).

(14) M. Eisenberg, C. W. Tobias and C. R. Wilke: Chem. Eng. Prog. Symp. Series, **51** (1953), 1.

(15) J. A. R. Bennet and J. B. Lewis: AIChE Journal, **4** (1958), 418.

(16) M. Umakoshi, K. Mori and Y. Kawai: J. Iron Steel Inst. Japan, **62** (1976), S570 (in Japanese).

(17) Y. Kawai: *Tetsuyakin-Hanno-Sokudo-Ron*, Nik-kan-Koogyo-Shinbun-Sha, (1973), p. 142 (in Japanese).

(18) T. K. Sherwood and J. M. Ryan: C. E. S., **11** (1959), 81.

(19) R. N. Smith and R. Greif: Trans. ASME, J. Heat Transfer, **97** (1975), 594.

(20) J. F. Elliot and M. Gleiser: Therm. Chemistry for Steelmaking, Addison-Wesley, Vol. I, (1960), 7.

(21) T. P. Yao and V. Kondic: J. Inst. Metals, **81** (1952/53), 17.

(22) K. Uemura: J. Iron Steel Inst. Japan, **25** (1939), 24 (in Japanese).

(23) Metal Handbook, 8th edition, ASM, (1973), 260.

(24) I. Cornett and R. Kappesser: J. Electrom. Soc., **118** (1971), 1957.

(25) R. A. Seban and H. A. Johnson: NASA Memorandom (1959), 4–22–59W.